Tidally-driven interannual variation in extreme sea level probabilities in the Gulf of Maine

H. E. Baranes[1], J. D. Woodruff[1], S. A. Talke[2], R. E. Kopp[3], R. D. Ray[4], and R. M. DeConto[1]

[1]Department of Geosciences, University of Massachusetts Amherst, Amherst, MA, USA, [2]Civil and Environmental Engineering Department, California Polytechnic State University, San Luis Obispo, CA, USA, [3]Department of Earth & Planetary Sciences and Institute of Earth, Ocean & Atmospheric Sciences, Rutgers University, New Brunswick, NJ, USA, [4]Geodesy and Geophysics Laboratory, NASA Goddard Space Flight Center, Greenbelt, MD, USA

Corresponding author: Hannah Baranes (hbaranes@geo.umass.edu)

Key Points:

- We present a new quasi-nonstationary joint probability method that estimates tidally driven interannual fluctuations in flood hazard
- This method provides more precise and stable storm tide probability estimates than extreme value distributions fit to measured storm tides
- In the Gulf of Maine, tides force decadal oscillations in the 1% probability storm tide at a rate exceeding mean historical sea-level rise

Abstract

Astronomical variations in tidal magnitude can strongly modulate the severity of coastal flooding on the daily, monthly, and interannual timescales. Here, we present a new quasi-nonstationary joint probability method (qn-SSJPM) that estimates interannual fluctuations in flood hazard caused by the 18.6 and quasi 4.4-year modulations of tidal properties. We demonstrate that the qn-SSJPM provides more precise and stable storm tide probability estimates compared with the standard practice of fitting an extreme value distribution to measured storm tides, which is often biased by the largest few events within the observational period. Applying the qn-SSJPM in the Gulf of Maine, we find significant tidal forcing of flood hazard by the 18.6-year nodal cycle, whereas 4.4-year modulations and a secular trend in tides are small compared to interannual variation and long-term trends in sea-level. The nodal cycle forces decadal oscillations in the 1% annual exceedance probability storm tide at an average rate of ±13.5 mm/y in Eastport, ME; ±4.0 mm/y in Portland, ME; and ±5.9 mm/y in Boston, MA. Currently, nodal forcing is counteracting the sea-level rise-induced increase in flood hazard; however, in 2025, the nodal cycle will reach a minimum and then begin to accelerate flood hazard increase as it moves toward its maximum phase over the subsequent decade. Along the world's meso-to-macrotidal coastlines, it is therefore critical to consider both sea-level rise and tidal non-stationarity in planning for the transition to chronic flooding that will be driven by SLR in many regions over the next century.

Plain Language Summary

Coastal management practices around flood risk often rely on estimates of the percent chance of a particular flood height occurring within a year. For example, U.S. flood insurance requires designating areas with a 1% annual flood probability (the "100-year flood zone"). When storms hit regions with large tides, the height and timing of high tide often determine flood severity. Thus, the relationship between flood height and annual probability can be altered by natural, daily-to-decadal cyclical variation in tide heights. Here, we present a new method for calculating annually-varying flood height–probability relationships based on known tidal cycles. Applying the new method in the Gulf of Maine, we find that an 18.6-year-long tidal cycle (the *nodal cycle*) forces decadal variation in the 1% annual probability flood at a faster rate than the historical average rate of sea-level rise over the past century. Currently, nodal cycle forcing is counteracting the sea-level rise-induced increase in flood hazard; however, in 2025, the nodal cycle will reach a minimum in the Gulf and then begin to accelerate flood hazard increase as it moves toward its maximum over the subsequent decade. It is therefore critical to consider sea-level rise and tidal variation in long-term flood hazard planning.

1 Introduction

Extreme sea levels (ESLs) pose a growing hazard to coastal communities (e.g. Hallegatte et al., 2013; Neumann et al., 2015). Coastal management practices around flood risk often require estimates of ESL annual exceedance probability (AEP), or the percent chance of an ESL occurring in a given year. In the United States, for example, federal flood insurance and building codes depend on estimates of the current 1% AEP flood zone (Galloway et al., 2006; Hunter, 2010; Buchanan et al., 2017). ESL hazard, however, is not stationary. The relationship between flood height and AEP is approximately log-linear, so even small interannual variations in storm surge, tides, waves, or mean sea-level (trends on the order of millimeters per year) can significantly alter ESL frequencies (e.g. Oppenheimer et al., 2019). Robust statistical methods for considering sea-level non-stationarity (Hunter, 2010; Buchanan et al., 2017; Wahl et al., 2017) have been used to incorporate uncertain sea-level rise (SLR) projections into global (e.g. Lin et al., 2016; Garner et al., 2017; Oppenheimer et al., 2019) and local (e.g. NYC, 2013; Douglas et al., 2016; Griggs et al., 2017) hazard assessments. In this paper, we investigate the impact of quasi-deterministic variation in astronomical tides on low-probability, high-impact ESLs.

Tidal magnitude modulates the severity of flooding in meso-to-macrotidal regions, and interannual variation in tides causing periods of enhanced flood risk is a well-known phenomenon (e.g. Eliot, 2010; Menéndez & Woodworth, 2010; Ray & Foster, 2016; Talke et al., 2018; Peng et al., 2019; Haigh et al., 2020; Talke & Jay, 2020). In particular, the 18.6-year lunar nodal cycle and the 8.85-year cycle of lunar perigee influence high water globally on weekly, monthly, and annual timescales (e.g., Haigh et al., 2011; Peng et al., 2019). Ray and Foster (2016) showed that the perigean cycle modulates predicted future nuisance tidal flooding at a quasi 4.4-year period. For extreme flooding, Menéndez and Woodworth (2010) modeled global nodal and perigean astronomical modulations using a non-stationary location parameter in ESL probability distributions fit to satellite altimetry records 1970 to 2008. Over a longer, nearly 200-year record from Boston, Massachusetts, Talke et al. (2018) also showed that the nodal cycle produces 10–20 cm of variation in ESLs with AEPs between 1% and 50%.

On decadal to centennial timescales, non-astronomical factors also force local-to-global-scale variations and trends in tides (Haigh et al., 2020; Talke & Jay, 2020). Changes in water depth, shoreline position, frictional resistance, and river flow have led to dramatic local-scale tidal amplification and reduction over the past two centuries, particularly in estuaries and tidal rivers (Winterwerp et al., 2013; Haigh et al., 2020; Talke & Jay, 2020). Spatially coherent, regional scale variation in tides has been driven by changes in ocean depth, shoreline position, sea ice extent, ocean stratification, non-linear interactions, and radiational forcing (e.g. Woodworth et al., 2010; Muller et al., 2011; Muller, 2012; Haigh et al., 2020).

In summary, interannual variations and long-term trends in tides have significant implications for flood hazard. Astronomical nodal and perigean cycles can significantly increase flood hazard compared to the long-term average during their positive phases (e.g. Talke et al., 2018), and secular changes in tides driven by non-astronomical factors will either enhance or counteract the increase in flood hazard driven by SLR (e.g. Haigh et al., 2020). Given that the probability of flooding changes year-to-year, considering sea-level rise and tidal non-stationarity together is important to both short and long-term municipal planning and emergency management at the coast. However, as mentioned by Talke et al. (2018), no method for assessing tidally driven interannual variation in ESL hazard has yet been developed. In this paper, we describe a new method for estimating tidally driven non-stationarity in ESLs, using an adaptation of the measurement-based joint probability methods developed by Pugh and Vassie (1978, 1980), Tawn and Vassie (1989), Tawn (1992), and Batstone et al. (2013). We apply and validate our methodology using century-long tide gauge records from the Gulf of Maine coast in the northwest Atlantic Ocean (Fig. 1), a region with significant tidal trends and nodal variability (Ray, 2006; Ray & Talke, 2019). Under the assumption of stationary storm characteristics, this new quasi-nonstationary joint probability method provides separate statistical treatment of tides and surge and accounts for interannual variation in tides.

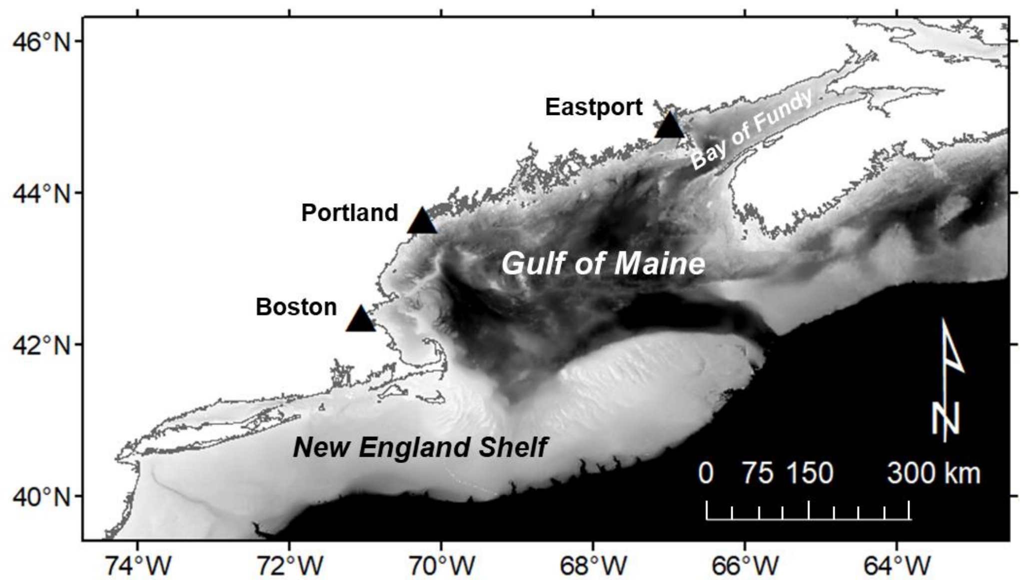

Figure 1. Gulf of Maine site map, including gauge locations mentioned in the text.

2 Background

2.1 Site description

We apply this new quasi-nonstationary joint probability method to estimating ESL probabilities at the three longest running and most complete National Oceanic and Atmospheric Administration (NOAA) tide gauge records within the Gulf of Maine at Boston, Portland, and Eastport (Fig. 1). Table 1 shows their locations, measurement timespans, and relevant tidal datums. An additional record at St. John, New Brunswick (1893-present) is not included because of significant data gaps and unusual interannual variation in the amplitude of the M_2 tidal constituent after 1980 (Ray & Talke, 2019). In addition to its multiple century-long tide gauge records, the Gulf of Maine's large tide range and known local and regional tidal variation make it an ideal location for applying our statistical method. The region also hosts major cities and sensitive infrastructure that require careful flood risk assessment; for example, Hallegate et al. (2013) ranked Boston, Massachusetts as being at risk to suffer the eighth and seventeenth highest flood losses in the world in 2005 and 2050, respectively.

The Gulf of Maine coast is vulnerable to flooding from both Tropical cyclones (TCs) and extratropical cyclones (ETCs), but ETCs have historically been the dominant flooding mechanism, as they are more frequent and more likely to intersect with high tide (e.g. Kirshen et al., 2008; Talke et al., 2018). The total still water level (i.e. not including waves) recorded during a storm, relative to some vertical datum, is called *storm tide* and represents the net impact of meteorological and tidal forcing. Here, we use annual mean sea level (MSL) as the vertical datum, such that storm tide time series do not include SLR. *Storm surge* is the meteorologically forced deviation from the predicted tide, calculated by subtracting the predicted tide from time series of measured storm tide values. Extreme storm surges reach ~1.3 m in the Gulf (e.g. Talke et al., 2018), and tides are significantly larger. The great diurnal tide range increases northward from 3.1 meters in Boston to ~16 meters in the Bay of Fundy's northern embayments, making tides a primary control on most of the region's extreme coastal flooding events. In Boston, for example, Talke et al. (2018) found that 92 of the top 100 storm events occurring between 1825 and 2018 coincided with a predicted high tide that exceeded modern mean higher high water.

Tides in the Gulf of Maine and Bay of Fundy are unusual in several respects. In addition to the well-known large tidal range, there is a natural resonance frequency in the Gulf near the frequency of the N_2 tide (Garrett, 1972; Godin, 1993). Observed N_2 amplitudes are larger than S_2 amplitudes, opposite of the tidal potential; thus, the classic fortnightly spring-neap modulation is relatively weak and is smaller than the monthly modulation induced by M_2/N_2 beating. The strongest astronomical tides during any month therefore occur near times of lunar perigee. Similar to many locations, there are additional modulations at semiannual, 4.4-year, and 18.6-year periods (Haigh et al., 2011; Ray & Merrifield, 2019). The 4.4-year and 18.6-year modulations of the highest predicted tide are moderate at Boston and Portland (roughly 3–4 cm in amplitude) but get much larger (up to 15 cm in amplitude) inside the Bay of Fundy (Ray & Merrifield, 2019). The 18.6-year modulation is caused by the lunar nodal cycle, or a precession of the moon's orbital plane around the ecliptic 360° every 18.6 years. The 4.4-year modulation is caused by perigean spring tides coinciding with the winter or summer solstice (when the diurnal tidal contribution is largest) twice per 8.85 years (see Ray & Foster, 2016 for an explanation).

Perhaps owing to the basin resonance being near N_2, Gulf of Maine tides are sensitive to small changes in basin geometry, depth, and friction. Indeed, they display some of the largest secular tidal trends observed anywhere in the world for a regional body of water. Since the early-20th century, the amplitude of the M_2 tidal constituent has increased at an average rate of 0.77 ± 0.08 mm/y at the Boston tide gauge, 0.59 ± 0.04 mm/y at Portland, and 0.25 ± 0.04 mm/y at Eastport (Ray & Talke, 2019). In comparison, rates of SLR measured at these tide gauges over the same time period are 2.83 ± 0.15 mm/y in Boston, 1.88 ± 0.14 mm/y in Portland, and 2.14 ± 0.17 mm/y in Eastport. New tide estimates derived from 19th-century water level measurements show that the M_2 trend began sometime in the late-19th or early-20th century, coincident with the transition to modern rates of SLR (Ray & Talke, 2019). Numerical models show that SLR has only caused part of the observed increase in M_2 amplitude in the Gulf of Maine (Muller et al., 2011; Greenberg et al., 2012; Schindelegger et al., 2018), suggesting that ocean stratification driven by sea-surface temperature warming has also played a role in the increase (Muller, 2012).

2.2 Review of ESL statistical methods

ESL AEPs can be estimated from data or models. In both cases, an extreme value probability distribution is fit to a set of measured or simulated ESLs assumed to be representative of the possible flood scenarios in a region. Hydrodynamic simulations have the advantage of providing spatially continuous flood elevations and flow velocities, but they are computationally intensive, take time to develop, and as with all models, rely on uncertain parameterizations, bathymetry, and assumptions (e.g. Vousdoukas et al., 2016; Lin et al., 2010). At gauged locations with multi-decadal records, estimating ESL AEPs from data is a simpler alternative that will be the focus of this paper.

The two most commonly used extreme value distributions are the Generalized Extreme Value distribution (GEV) and the Generalized Pareto Distribution (GPD). The GEV is fit to block maxima data, or the n-largest measurements per some time interval (e.g. the largest event each year), and the GPD is fit to peaks-over-threshold data, or all measurements over some threshold value. The GPD approach is more robust because it uses more available extreme observations (e.g. NERC, 1975; Coles et al., 2001; Tebaldi et al., 2012; Buchanan et al., 2017). In Boston, for example, only 46 of the top 100 storm tides recorded at the NOAA gauge occurred in distinct years, and a GEV using annual block maxima would therefore omit more than half of the top-100 events. Compared with the GEV, however, the GPD requires higher data quality and is more difficult to fit automatically because of its sensitivity to the choice of threshold (Coles, 2001; Arns et al., 2013). ESL statistics published by NOAA, for example, are derived from GEV fits because choosing a GPD threshold can be subjective, and NOAA requires a method that can be quickly applied and periodically updated at over 100 gauges (Zervas, 2013). Nonetheless, a comparison of GEV and GPD fits to Boston extreme storm tides yielded similar AEP estimates (Talke et al., 2018).

In meso-to-macrotidal regions, where tides are a primary control on flooding, a joint probability approach that convolves separate tide and surge distributions can capture more extreme storm surges within a temporally limited tide gauge record (e.g. Pugh & Vassie, 1979, 1980). For example, in 63 of the 100 years in Boston's record, the largest storm surge of the year did not coincide with any of the year's top-3 storm tides; thus, a GPD fit to measured Boston storm tides would exclude two-thirds of the largest storm surges (assuming a GPD threshold that was exceeded, on average, three or fewer times per year). The first two published ESL joint probability methods were the Joint Probability Method (JPM; Pugh & Vassie, 1978, 1980) and the Revised Joint Probability Method (RJPM; Tawn & Vassie, 1989; Tawn, 1992). The JPM separates measured water levels into the predicted tide and a non-tidal residual (measured minus predicted water level at a given time), fits an empirical probability distribution to each component, and obtains the joint ESL distribution by a convolution of the two component distributions. The RJPM improves upon the JPM by 1) fitting a GEV distribution to extreme non-tidal residual values in order to model events exceeding the observed maximum, and 2) applying an extremal index that accounts for dependence of non-tidal residuals occurring close together in time (the extremal index will be further explained in section 3.2).

The primary shortcoming of the JPM and RJPM is the assumed independence between the predicted tide and the non-tidal residual. Storm surge and tides interact; storm surge increases water depth, and tidal wave speed increases in deeper water (Horsburgh and Wilson, 2007). The non-tidal residual time series of measured minus predicted water level therefore often includes an "illusory" surge during storm events, which is an artifact of the difference in the predicted tide and the phase-shifted tide. Furthermore, the amplitude, timing, and timescale of the surge wave impacts its frictional interaction with tides (Familkhalili et al., 2020).

The Skew Surge Joint Probability Method (SSJPM; Batstone et al., 2013) improves upon the JPM method by eliminating the bias introduced by the uncertain timing of the tidal prediction during storm conditions. *Skew surge* is defined as the difference between the maximum measured water level and the predicted high water within each tidal cycle. Williams et al. (2016) found statistical independence between predicted high water and skew surge at 77 Atlantic tide gauges in the United States and Europe. They concluded that this skew surge independence enables a simplified joint probability approach for calculating ESL AEPs that does not require the inclusion of an empirical relationship between tide and the non-tidal residual to account for tide-surge interaction. The argument is primarily statistical and not dynamical, as the absence of correlation does not indicate the absence of effect; rather, in observational records, natural variability in storm systems dominates over tidally driven variation in surge. We address this issue by using primarily coastal, and not estuary, locations, such that frictional interaction effects are likely less prominent.

These joint probability methods have lowered bias in ESL AEP estimates (compared to GPD or GEV fits to data) in regions where tides are large relative to meteorological forcing, particularly for short data series (Dixon & Tawn, 1999; Haigh et al., 2010); however, none has accounted for year-to-year fluctuations or secular trends in tidal properties. In the following sections, we describe a new, quasi-nonstationary (*qn*) modification of the SSJPM called the *qn-SSJPM*, which calculates a separate set of ESL AEPs for winter and summer storm seasons using that season's known high tides. We fit separate summer and winter distributions because the region's large storm events mostly occur in the winter season (e.g. Talke et al., 2018), while summertime tides are larger on average (Ray & Foster, 2016).

3 Methods

3.1 Tide gauge data processing

At the Eastport, Portland, and Boston NOAA gauges, we use hourly water level data from NOAA, downloaded from the University of Hawaii Sea Level Center database for pre-2016 data (Caldwell et al., 2010) and from NOAA's website for post-2016 data (https://tidesandcurrents.noaa.gov). We remove the annual MSL trend by subtracting a one-year moving average of all hourly water level measurements (following Arns et al., 2013).

We fit a six-minute cubic spline function to the hourly data (six-minute data are only available from NOAA beginning in 1996) to reduce the peak truncation caused by using hourly records. For example, hourly-based high waters from Boston in 2018 were an average of 4.1 cm lower than 6-minute resolution records, and the six-minute spline fit reduces this bias to 0.7 cm. Since the precision of individual, pre-digital measurements varies from 0.015 m(due to rounding) to 0.05–0.1 m or more during periods with timing or gauge problems (e.g., Talke et al., 2018, 2020), this small bias is less than other sources of error. An alternate, bias-free approach (used by Talke et al. 2018) is to use the monthly maxima water levels tabulated by NOAA; however, this approach precludes the use of two or more maxima that occur within a month. For all these reasons, all subsequent calculations use this MSL-adjusted six-minute spline fit to the hourly data.

We estimate the tidal contribution to each water level measurement using the MATLAB-based harmonic analysis program r_t_tide (Pawlowicz et al., 2002; Leffler and Jay, 2009). We calculate tidal constituents independently for each year from a 369-day analysis that includes 67 constituents. The 369-day analysis enables estimation of the semiannual and annual constituents, as well as the seasonal sidelines to M_2 (often called MA_2 and MB_2, but labeled H_1 and H_2 in r_t_tide). Since we are interested in the effect of the nodal cycle, no nodal corrections were applied. r_t_tide also applies nodal corrections based on the astronomic potential, rather than the empirically measured and slightly smaller correction observed in practice (e.g. Ku et al., 1985; Ray & Foster 2016; Ray & Talke, 2019).

We calculate the skew surge parameter by subtracting maximum predicted water level from maximum observed water level within each tidal cycle. Following Williams et al. (2016), we test for statistical independence between predicted high water and the top 1% of skew surge at all sites using the rank-based Kendall's Tau correlation test (Kendall, 1938), where the criteria for significant correlation are $|tau| > 0.1$ and $p < 0.05$. We do not find significant correlation between predicted high water and skew surge at any of the three sites (Tab. 2).

Prior to the joint probability analysis, we divide tides and skew surges into the winter storm season (defined as 31 October to 30 April) and the more quiescent summer season (1 May to 30 October) Wahl and Chambers, 2015; Thompson et al., 2013). Including 31 October in the winter storm season avoids exclusion of a 1991 storm (Talke et al., 2018). In all subsequent analyses, we only include seasons where the set of measured water levels is at least 75% complete (Menéndez and Woodworth, 2010; Wahl and Chambers, 2015).

3.2 Quasi-nonstationary joint probability analysis (qn-SSJPM)

Each winter or summer ESL distribution is calculated by convolving probability distributions of that season's predicted high waters and all winter or summer skew surges recorded over the length of the tide gauge record. We model winter and summer extreme skew surge probabilities with a GPD, following Batstone et al., (2013). For skew surges above a threshold μ, the GPD cumulative distribution function (CDF) $G_{ss}(x)$ takes the form

$$G_{ss}(x) = 1 - \left(1 + \xi \frac{x - \mu}{\sigma}\right)^{-1/\xi} \quad (1)$$

with shape parameter $\xi \neq 0$ and scale parameter $\sigma > 0$. To account for uncertainty in the skew surge GPD, we sample 1,000 pairs of ξ and σ from the covariance matrix of their maximum likelihood estimates with Latin hypercube sampling (Buchanan et al., 2016, 2017). We choose the GPD threshold that defines extreme skew surges by minimizing the root mean square error of the GPD versus the empirical distribution $\tilde{F}_{ss}(x)$ (commonly called the plotting position; Arns et al., 2013). We calculate empirical AEPs using the Weibull formula

$$\tilde{F}_{ss}(x_i) = \left(\frac{n}{num\_yrs}\right)\left(\frac{i}{n+1}\right) \quad (2)$$

where *i* is the rank of event *x*, *n* is the total number of events, and *num_yrs* is the number of years in the record. We find that setting the threshold as the 99.7th percentile of skew surges for both the winter and summer seasons minimizes error across all sites, and past studies have used a similarly high threshold (Menéndez and Woodworth, 2010; Arns et al., 2013). This 99.7th percentile threshold samples an average of 1.1 events per season. Following Batstone et al. (2013), we assume there are sufficient observations to use the empirical distribution $\tilde{F}_{ss}(x)$ (equation 2) for skew surges below the threshold, such that the CDF of all skew surges $F_{ss}(x)$ is

$$F_{ss}(x) = \begin{cases} \tilde{F}_{ss}(x), & x < \mu \\ (1 - 0.997) * G_{ss}(x) + 0.997, & x \geq \mu \end{cases} \quad (3)$$

We then calculate the joint CDF of storm tides $F_{ST}(x)$ for each season following the SSJPM (Batstone et al., 2013), which assumes that there is an equal probability of a given skew surge occurring at any high tide in a season:

$$F_{ST}(x) = \left[\prod_{t=1}^{N} F_{ss}(x - P_t)\right]^{1/N} \quad (4)$$

where P_t is the predicted high water in tidal cycle t, and N is the total number of high waters in the season. To account for statistical uncertainty in the skew surge GPD parameters, tides are convolved with all 1,000 skew surge GPDs (F_{ss}). The 50th quantile of the resulting 1,000 storm tide distributions (F_{ST}) represents the central estimate, and the 5th and 95th quantiles provide a 90% uncertainty range. We convert storm tide cumulative probabilities to AEPs by

$$AEP(x) = [N * \theta(x)] * [1 - F_{ST}(x)] \quad (5)$$

where $\theta(x)$ is the extremal index, which effectively reduces the number of high waters per season to the number of independent high waters per season to account for events that span multiple high tides (Leadbetter, 1983; Tawn, 1992). The extremal index is the inverse of mean cluster size (the mean number of storm tides exceeding a certain height that are associated with a single event) and calculated as a function of storm tide, following Ferro and Segers (2003):

$$\frac{1}{\theta(x)} = \frac{2\left[\sum_{i=1}^{E(x)-1}(I(x)_i - 1)\right]^2}{(E(x)-1) * \sum_{i}^{E(x)-1}[(I(x)_i - 1) * (I(x)_i - 2)]} \quad (6)$$

where *E(x)* is the number of measured storm tides exceeding *x*, and *I(x)* is interexceedance time. We find that the extremal index reduces storm tide magnitudes in the 1 to 30-year return period (~3 to 100% AEP) range; thus, it is likely that these water levels are sometimes exceeded multiple times during a single storm event, while the most extreme water levels with AEPs less than 3% are generally independent.

At each site, the final products of the qn-SSJPM calculations include:

1. An ESL AEP curve for each summer and winter season
2. Annual ESL AEP curves, calculated by adding the expected number of summer and winter exceedances in a given year for each storm tide height (where, for example, 10% AEP = 0.1 expected exceedances per year)
3. Two time-integrated ESL AEP curves (one winter, one summer), calculated using winter or summer tides over the full length of the historical record
4. A combined winter-summer, time-integrated ESL AEP curve

4 Results and discussion

4.1 qn-SSJPM results and validation

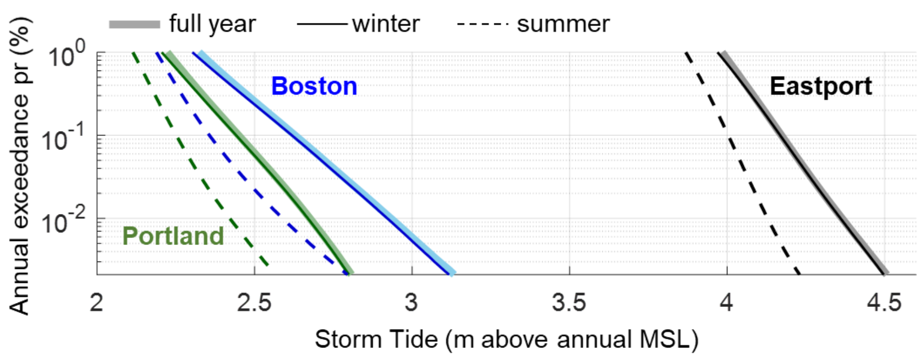

Figure 2. Seasonality of Gulf of Maine flood hazard. Historical time-integrated qn-SSJPM ESL AEP curves for the winter season (thin solid lines), summer season (dashed lines), and full year (thick solid lines) at Eastport (black), Portland (green), and Boston (blue).

We focus our discussion on winter storm season results because extreme flooding is primarily a winter hazard in the Gulf of Maine. A comparison of the historical time-integrated qn-SSJPM ESL AEP curves for winter, summer, and the full year (Fig. 2) shows that storm tides from the full-year curves are, at most, 1.5 cm higher than winter curves at AEPs below 10%. Thus, when viewing the full-year curve, it is important to do so with the caveat that summer floods are only a minor contributor to total flood hazard.

Figure 3 shows the historical annual and time-integrated winter-season ESL AEP curves for Eastport, Portland, and Boston. The spread among annual curves represents deterministic tidal variability and is thus greatest in Eastport where tide range and nodal cycle amplitude are the largest; for example, depending on the year, 1% AEP winter storm tides range 4.20–4.50 m in Eastport, 2.56–2.74 m in Portland, and 2.83–2.99 m in Boston (all storm tides are relative to annual MSL). The 90% uncertainty region (blue shading in Fig. 3) encompasses both deterministic tidal variability and statistical uncertainty in the skew surge GPD parameters.

We also compare qn-SSJPM ESL AEP distributions to a GPD fit to the top 0.3% of storm tides in each record (Fig. 3). This is a common approach for deriving ESL AEPs (see section 2.2), hereafter referred to as GPD_{ST}, and we fit GPD_{ST} following the same methods described in section 4 for fitting the skew surge GPD. In Boston, the GPD_{ST} method estimates significantly higher winter storm tides at AEPs <10% compared to the qn-SSJPM. Given the disagreement, we test the two statistical approaches using a Monte Carlo validation. We create a 10,000-year synthetic time series of winter-season high waters by splicing together the 1921-2018 Boston winter-season predicted high waters 102 times (102 times the 98-year record ≈ 10,000 years) and combining each predicted high water with a skew surge randomly sampled from the CDF of Boston winter skew surge probabilities.

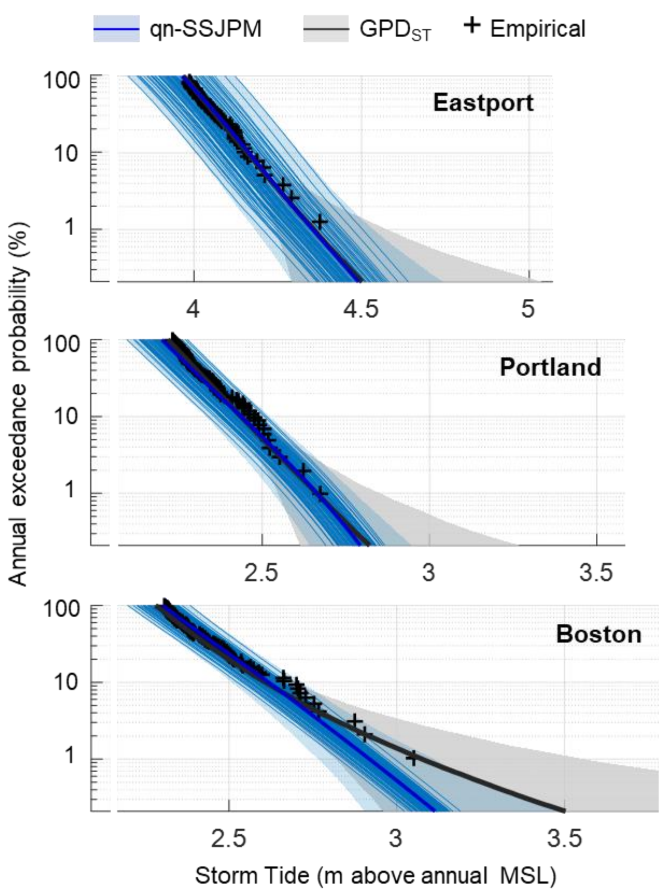

Figure 3. Comparison of winter-season ESL AEP curves for the qn-SSJPM and a GPD fit to measured storm tides. Thin blue curves show qn-SSJPM-derived curves for each winter storm season in the tide gauge record, and bold blue curves are the time-integrated qn-SSJPM curves based on the entire tide gauge record. Black curves are a GPD fit to the top 0.3% of storm tides in each tide gauge record (GPD_{ST}), and + signs are empirical AEPs (see equation 2). Lines represent central estimates (50th quantile), and filled regions show the 90% uncertainty range (5th–95th quantiles) for each method.

We treat empirical ESL AEPs calculated from the 10,000-year record (using equation 2) as the "truth." We then run 1,000 trials of randomly selecting 100 of the 10,000 years and calculating ESL AEP distributions with a 67% uncertainty range for those 100 years using both the qn-SSJPM and GPD_{ST} methods. We use the 99.7th percentile storm tide and skew surge as

GPD thresholds, and for the qn-SSJPM calculation, we only generate a single time-integrated ESL AEP distribution for the 100 years (i.e. we do not calculate annual distributions). For each trial, we then determine 1) whether or not the truth (based on empirical AEPs) falls within the central 67% ranges of the 10%, 1%, and 0.2% storm tide estimates for the two methods, and 2) the bias of the estimates, calculated as the difference between the truth and the central qn-SSJPM and GPD_{ST} estimates of the 10%, 1%, and 0.2% AEP storm tides.

We find that the synthetically-generated truth falls within the central 67% range of estimates 55–65% of the time for the qn-SSJPM and 59–67% of the time for GPD_{ST} (Fig. 4a). Both methods' overlap with the truth generally increases for lower-AEP storm tides because uncertainty range also increases with decreasing AEP. The lower coverage of qn-SSJPM error ranges indicates that the method's estimate errors are more overconfident than GPD_{ST} estimate errors; however, both the qn-SSJPM and GPD_{ST} have reasonable coverage.

Comparing biases in qn-SSJPM and GPD_{ST} estimates of the 10%, 1%, and 0.2% AEP storm tides reveals that qn-SSJPM estimates are more precise and stable (i.e. consistently closer to the truth). Box plots in Figure 4b show the each method's biases for all 1,000 trials. The interquartile ranges increasing (i.e. the boxes getting larger) at lower AEPs reflects the expected trend of AEP estimate instability (i.e. variability) increasing at lower AEPs for a given record length (e.g. Haigh et al., 2010). Mean bias is close to zero for both methods at all three AEPs; however, for the 1% and 0.2% AEP storm tides, both the interquartile range and total range in biases is significantly narrower for the qn-SSJPM estimates compared to GPD_{ST} estimates. This result indicates that for a 100-year observational record, both methods will, on average, provide accurate ESL estimates for storm tides with AEPs between 0.2 and 10%; however, GPD_{ST} estimates of storm tides with return periods nearing the record length (e.g. the 100-year return period or 1% AEP storm tide for a 100-year-long record), are more susceptible to being biased by the largest few events within the observational period. This finding is consistent with past studies that have shown GPD and GEV fits to observed storm tides (often called "direct methods" of estimation) are more unstable to historical outlier events than joint probability distributions that incorporate large historical storm surges that did not necessarily coinciding with high tides (e.g. Tawn and Vassie, 1989; Tawn, 1992; Haigh et al., 2010).

This instability to historical outliers partially explains the disagreement between the qn-SSJPM and GPD_{ST} curves for Boston (Fig. 3). Boston's highest three recorded flood events all occurred in years with unusually large tides (Talke et al., 2018). For example, the Blizzard of 1978 (the storm tide of record), happened to coincide with the year that, on average, had the largest-magnitude high waters over the past century (represented by the right-most blue curve in Fig. 3). Thus, the GPD_{ST} method in part overestimates Boston flood hazard because it does not account the Blizzard of 1978's 3.05-meter flood having had a lower probability of occurrence during any of the other 97 winters of record.

Comparing our Boston qn-SSJPM and GPD_{ST} winter ESL AEP curves to the to the Talke et al. (2018) flood frequency curve also highlights the influence of the most extreme historical events on the GPD_{ST} method (Fig. 5). Talke et al. (2018) reconstructs 200 years of Boston water levels 1825–2018 and fits a GPD to measured winter high waters (red curve in Fig. 5). This extended record includes three additional storm tides in 1830, 1851, and 1909 that nearly equal or exceed the 2018 storm tide (the second-highest within the NOAA record after the Blizzard of 1978). These additional storms lead to a GPD_{ST} fit that is more consistent with the qn-SSJPM fit, as indicated by the similarity of the blue and red curves in Fig. 5. Talke et al. (2018) also uses a higher GPD_{ST} threshold of 2.4 meters, compared to our 99.7th-percentile threshold of 2.31

meters. Re-calculating the GPD_{ST} curve for the 1925-2018 NOAA data with a 2.4-meter threshold produces a significantly different result compared to the 2.31-meter threshold (gray dashed line, compared to gray solid line in Fig. 5). This sensitivity to threshold selection highlights one of the key challenges in relying on a GPD fit to storm tides (e.g. Arns et al., 2013).

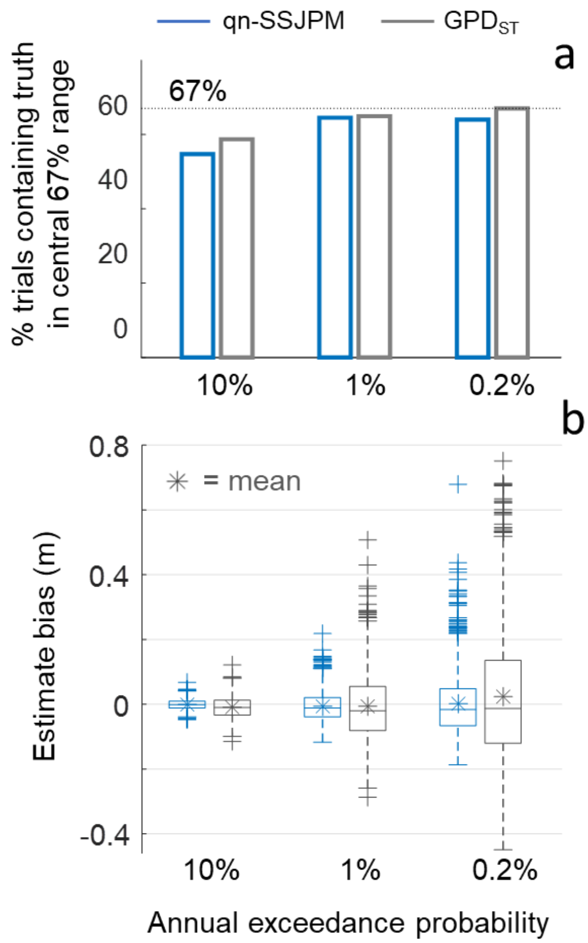

Figure 4. Validation results. *(a)* Percent of the 1,000 validation trials that contain the truth (empirical value) within the central 67% range of the 10%, 1%, and 0.2% AEP storm tide estimates for the qn-SSJPM method (blue) and the GPD_{ST} method (gray). *(b)* Box plot showing the distribution of qn-SSJPM and GPD_{ST} biases for the 1,000 validation trials at the 10%, 1%, and 0.2% AEP levels. Biases are calculated as the difference between the truth (based on the empirical distribution calculated from the 10,000-year synthetic record) and the central qn-SSJPM estimates (blue) or GPD_{ST} estimates (gray). Central marker is the median (with the * symbol showing the mean), and bottom and top box edges are the 25th and 75th quartiles. Values plotted as outliers (+ markers) fall outside the central 99.3% range.

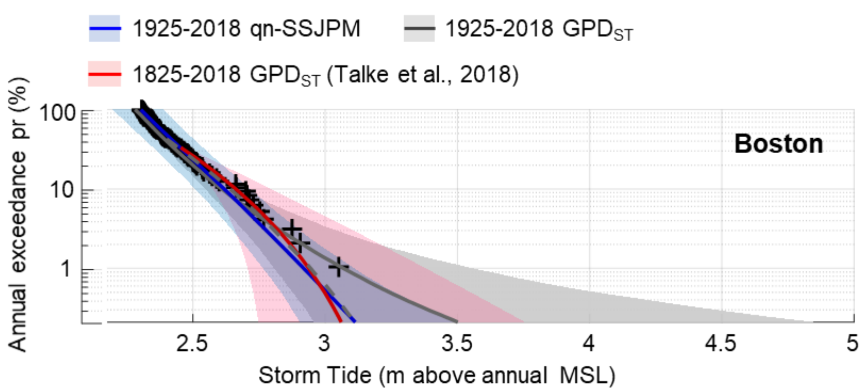

Figure 5. Comparison of Boston ESL AEP estimates. Curves represent the following distributions: (blue curve) time-integrated qn-SSJPM for 1925-2018; (solid gray curve) GPD fit

to measured storm tides (GPD_{ST}) for 1925-2018, calculated with 2.31-m (99.7th percentile) threshold; (gray dashed curve) same as solid curve, but calculated with Talke et al. (2018) 2.4-m threshold; (red curve) 1825-2018 Talke et al., (2018) ESL estimates (calculated using GPD_{ST} method with a 2.4-m threshold); (+ signs) empirical AEPs. Solid curves are central estimates, and filled regions show 95% uncertainty ranges.

4.2 Interannual variation in ESL probabilities

Interannual variation in tides forces changes flood hazard on annual-to-decadal timescales that should be considered in coastal management practices tied to ESL AEP estimates. We quantify the tidal modulation of flood hazard using the time series of winter storm season 1% AEP storm tides (hereafter referred to as $ST_{1\%}$) over the past century (Fig. 6). To represent the three dominant sources of interannual tidal variability in the region (see Ray & Foster, 2016), we fit a harmonic function to the time series with an 18.6-year period, a 4.4-year period, and a linear trend, where $ST_{1\%}$ values are relative to annual MSL, so the linear trend is the increase in tides above SLR. The ranges (twice the amplitudes) of the 18.6 and 4.4-year harmonics represent the magnitudes of the tidal cycles' forcing of flood hazard. Table 3 compares 18.6 and 4.4-year modulations of $ST_{1\%}$ and of the highest predicted tide (the highest tide in a 6-month interval), which are computed directly from harmonic constants at the gauges. The 18.6 and 4.4-year cycles' forcing of $ST_{1\%}$ is perhaps smaller than that of the highest predicted tide because $ST_{1\%}$ is calculated from observations rather than predictions. Observed water level data include atmospheric effects, which introduce variability that could interfere with tidal modulations. The exclusion of summer-season tides in the winter $ST_{1\%}$ values also likely reduces 4.4-year periodicity in predicted water levels (e.g. Talke et al., 2018).

The secular increase in tides observed in the M_2 tidal constituent (e.g. Ray & Talke, 2019) has driven roughly a 0.6 mm/y increase in $ST_{1\%}$ in Eastport and Portland. In Boston, however, there is a slight negative linear trend in $ST_{1\%}$ of -0.08 mm/y. Thus, the increase in tides has had a minimal decadal-timescale impact on $ST_{1\%}$ compared to other forcings; however, in Eastport and Portland, the total secular increase in $ST_{1\%}$ over the length of the tide gauge record is comparable to nodal variability. There is likely to be a future increase in high water levels with SLR (Greenburg et al., 2012; Pelling & Green, 2013; Schindelegger et al., 2018) and increasing tidal range (Greenberg et al., 2012), but there are no detailed projections for Gulf of Maine tides that consider additional forcing mechanisms, such as changes in stratification and flooding (Haigh et al., 2020).

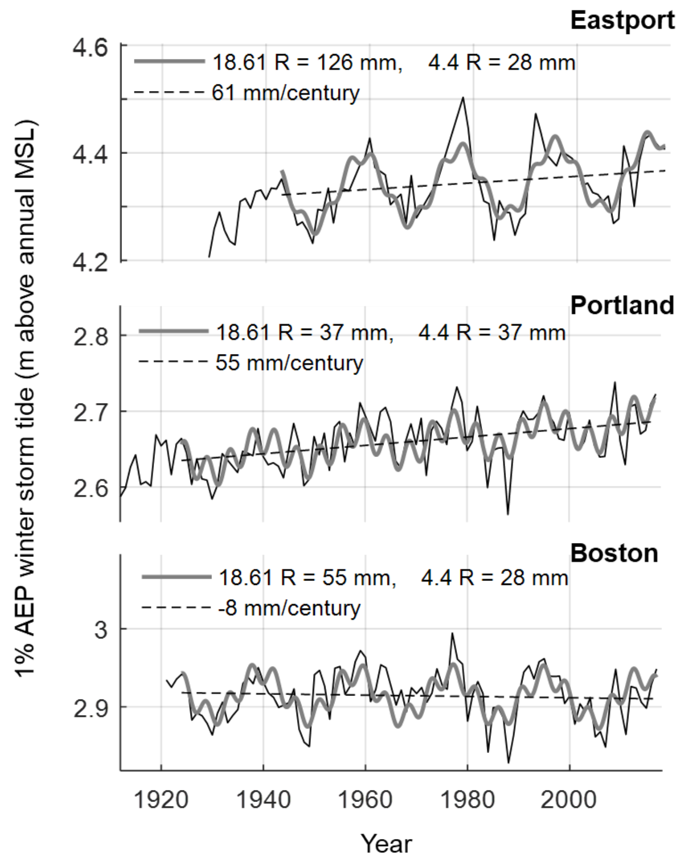

Figure 6. Interannual variation in the 1% AEP winter storm tide. Time series of the qn-SSJPM derived annual 1% AEP winter storm tide values (black line) with a least squares best-fit harmonic function that represents the region's dominant tidal forcings (gray curve), which includes an 18.6-year period, a 4.4-year period, and a linear trend. Legends show the ranges (i.e. double the amplitude) of the best-fit sinusoids and the slopes of the linear trends.

The significance of the 4.4 and 18.6-year tidal modulations of $ST_{1\%}$ can best be illustrated by converting the tidal cycle forcing ranges to rates and comparing them to rates of SLR. In Eastport, for example, the average range in 18.6-year forcing of $ST_{1\%}$ is 126 mm (Fig. 6). The 18.6-year forcing can be positive or negative, so over any half nodal period in Eastport, the average rate of nodal forcing of $ST_{1\%}$ is ±126 mm per 9.3 years, or ±13.5 mm/y. Applying the same calculation to Portland and Boston, the average 18.6-year tidal forcing rates are ±4.0 mm/y and ±5.9 mm/y, respectively. 4.4-year tidal forcing rates are a slower ±3.0 mm/y in Eastport and Boston and ±4.0 mm/y in Portland. In practice, however, interannual variation in winter MSL (which has historically been on the order of tens of mm) would drown out this shorter-period 4.4-year tidal modulation.

Figure 7 provides a visualization of the impact of 18.6-year forcing in the context of SLR. Historically at the three Gulf of Maine sites, on decadal timescales, the natural variability in $ST_{1\%}$ (and therefore flood hazard) driven by the nodal cycle has been larger than non-stationarity driven by the ~100-year average rate of SLR (black triangles versus asterisks in Fig. 7). In the future, even as SLR accelerates to equal or exceed rates of $ST_{1\%}$ nodal modulation, the nodal cycle will continue to force significant decadal-scale variability in the rate of flood hazard increase. We illustrate this effect through 2100 by adding the $ST_{1\%}$ nodal forcing rate to the projected mean rate of SLR over 9.3-year periods when nodal forcing will be trending positively (i.e. moving from a minimum toward a maximum). Over 9.3-year periods when the nodal cycle will be trending negatively, we subtract nodal forcing from projected SLR. We use Kopp et al. (2014) probabilistic local SLR projections, but we modify the ice sheet contributions by replacing the Church et al. (2013) likely ranges with Oppenheimer et al. (2019) likely ranges.

The nodal cycle is currently in its negative phase in the Gulf, and until it reaches its minimum in 2025, negative nodal forcing will counteract the SLR-induced increase in flood hazard. Between 2025 and 2034 (and in all decades when the nodal cycle is moving from a minimum to a maximum), however, positive nodal forcing will accelerate the flood hazard increase. Thus, it is critical to consider SLR and nodal cycle forcing together in planning for the transition to chronic flooding that will be driven by SLR in many coastal regions over the next century (e.g. Ray & Foster, 2016; Buchanan et al., 2017; Kopp et al., 2017; Talke et al., 2018; Oppenheimer et al., 2019).

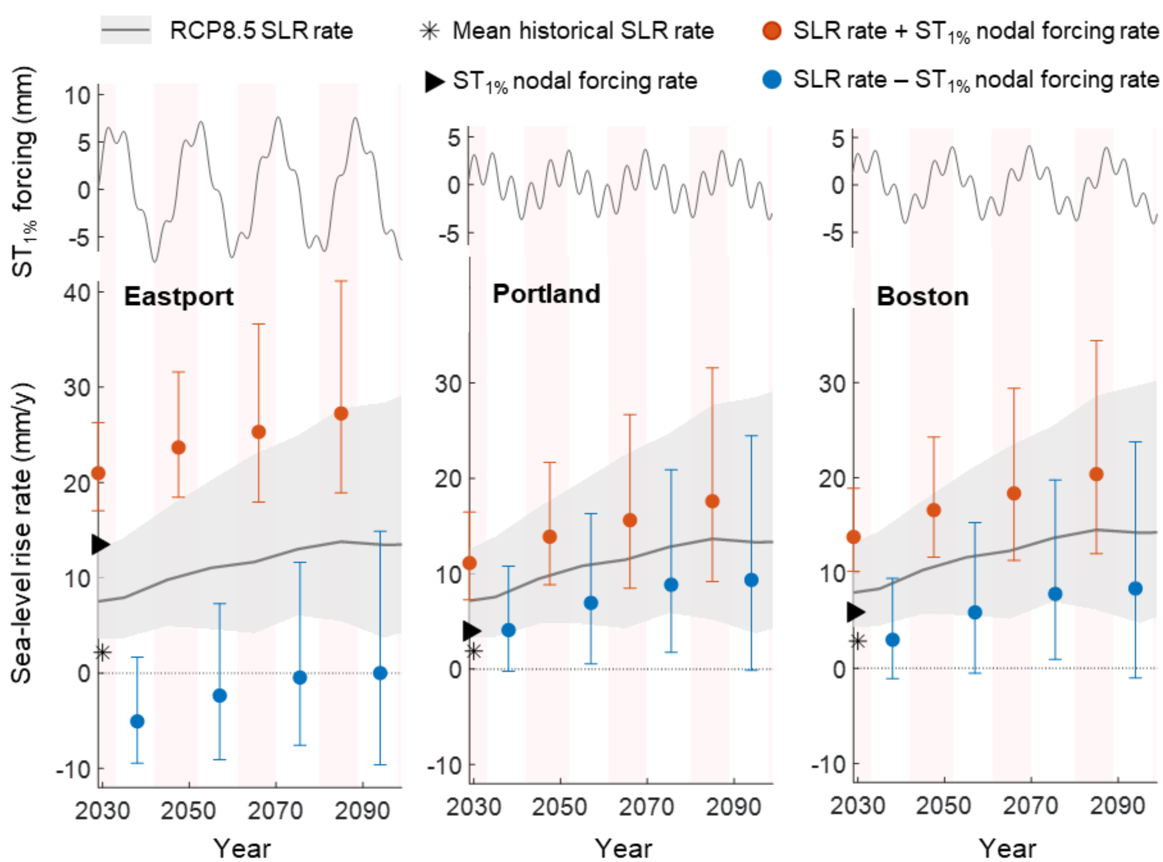

Figure 7. Joint impact of tidal forcing and sea-level rise on future flood hazard increase. *(Top panel)* 18.6 and 4.4-year components of the best-fit harmonic function to the winter $ST_{1\%}$ time series from Fig. 6. *(Bottom panel)* Gray curves show projected rates of local RCP8.5 SLR modified from Kopp et al. (2014) (line = 50^{th} quantile of samples, shading = central 90% range). Over 9.3-year-intervals where the nodal cycle is moving from a minimum to a maximum (indicated by red shading), the average nodal forcing rate (black triangle on y-axis) is added to the average projected rate of SLR over the same 9.3 years (red circles, with bars representing SLR uncertainty). Over intervals when the nodal cycle is trending negatively, nodal forcing is subtracted from the rate of SLR (blue circles and bars). The historical rate of SLR over the past century is also shown for reference (black asterisk on the y-axis).

4.3 Limitations

We demonstrate that the qn-SSJPM provides more precise and stable ESL AEP estimates than a GPD fit to measured storm tides. However, there are sources of uncertainty in the method, and there are additional forcings of interannual ESL variation that we do not account for. The skew surge GPD is a significant source of uncertainty, as GPD parameters are sensitive to both the choice of threshold (e.g. Coles, 2001; Arns et al., 2013) and the largest observed skew surge values (e.g. Tawn and Vassie, 1989; Tawn, 1992; Haigh et al., 2010). Furthermore, the accuracy of skew surge values depends on the accuracy of tidal predictions. The r_t_tide software does not include minor constituents (for example, our Boston r_t_tide predictions use 67 constituents, compared to the 108 used by Ray and Foster, 2016), and our calculations do not include tide prediction errors. The errors, however, are small; for example, M_2 amplitude errors are on the order of 0.1%.

The qn-SSJPM also does not incorporate climatic variability that may impact ESL hazard relative to annual MSL. For example, the North Atlantic Oscillation drives interannual variation in New England sea levels via northeasterly wind stress anomalies on the upper ocean (Goddard et al., 2015). In the future, increasing sea surface temperatures and changing atmospheric circulation patterns may also drive changes in storm intensity and frequency, but there is low confidence in site-specific projections of future storm behavior (e.g. Knutson et al., 2010; Emanuel et al., 2013), making it difficult to incorporate storm non-stationarity into flood hazard assessment. Finally, the qn-SSJPM does not consider the impact of wave processes on flood hazard. Wave set-up can be a significant contributor to flooding (e.g. Wolf, 2008, 2009), but tide gauges are generally established in sheltered embayments and therefore do not include wave set-up in their water level measurements.

5 Conclusions

We present a new quasi-nonstationary joint probability method for calculating ESL AEPs (the qn-SSJPM) and apply it along the Gulf of Maine coast, where tides are large and vary year-to-year. In addition to providing separate statistical treatment of tides and surge, the qn-SSJPM calculates distinct annual ESL hazard curves that account for interannual variation in tides. Each year’s ESL hazard curve is a convolution of 1) predicted high water probabilities, which are known based on that year’s tide predictions, and 2) skew surge probabilities determined from a GPD fit to all skew surges recorded over the length of a tide gauge record.

We use a Monte Carlo validation to compare the qn-SSJPM to the commonly used method of fitting a GPD to times series of measured storm tides. We find that the qn-SSJPM provides more precise and stable ESL AEP estimates because it is less susceptible to being biased by the largest few events within the observational period. At the three Gulf of Maine sites, we also find that interannual variation in tides significantly impacts design-relevant ESLs, such as the 1% AEP winter storm tide ($ST_{1\%}$). The 18.6-year nodal cycle forces decadal oscillations in $ST_{1\%}$ at a rate of 13.5 mm/y in Eastport, 4.0 mm/y in Portland, and 5.9 mm/y in Boston. In comparison, the average historical rate of local SLR over the past century has been between 1.89 and 2.86 mm/y at the three sites. Nodal forcing is currently counteracting the SLR-induced increase in flood hazard; however, in 2025, the nodal cycle will reach a minimum and then begin accelerating flood hazard increase as it moves toward its maximum phase over the subsequent decade.

SLR is driving a transition to severe chronic flooding in many coastal regions (e.g. Oppenheimer et al., 2019). Flooding becomes severe when water elevations cross thresholds defined by local topography and flood defense structures. The nodal cycle entering a positive phase my drive flood heights above these thresholds sooner than SLR would alone. Thus, considering tidal non-stationarity and SLR together is key to long-term municipal planning and emergency management along meso-to-macrotidal coastlines.

Acknowledgments and Data

H.E.B. was supported by the National Aeronautics and Space Administration (Award NNX16AO24H). Tide gauge data sources are described in the text, and the tidal prediction code sources are in the references. *[We will clean, comment, and upload MATLAB code to Zenodo if article is accepted and after revisions are made. For now, our code is attached to this submission as supplemental information files.]*

References

Arns, A., Wahl, T., Haigh, I. D., Jensen, J., & Pattiaratchi, C. (2013). Estimating extreme water level probabilities: A comparison of the direct methods and recommendations for best practise. *Coastal Engineering*, *81*, 51–66. https://doi.org/10.1016/j.coastaleng.2013.07.003

Batstone, C., Lawless, M., Tawn, J., Horsburgh, K., Blackman, D., McMillan, A., Worth, D., Laeger, S., & Hunt, T. (2013). A UK best-practice approach for extreme sea-level analysis along complex topographic coastlines. *Ocean Engineering*, *71*, 28–39. https://doi.org/10.1016/j.oceaneng.2013.02.003

Buchanan, M. K., Kopp, R. E., Oppenheimer, M., & Tebaldi, C. (2016). Allowances for evolving coastal flood risk under uncertain local sea-level rise. *Climatic Change*, *137*(3), 347–362. https://doi.org/10.1007/s10584-016-1664-7

Buchanan, M. K., Oppenheimer, M., & Kopp, R. E. (2017). Amplification of flood frequencies with local sea level rise and emerging flood regimes. *Environmental Research Letters*, *12*(6), 064009. https://doi.org/10.1088/1748-9326/aa6cb3

Caldwell, P. C., Merrifield, M. A., & Thompson, P. R. (2010). *Sea level measured by tide gauges from global oceans as part of the Joint Archive for Sea Level (JASL) since 1846* [Data set]. National Oceanographic Data Center, NOAA. https://doi.org/10.7289/V5V40S7W

Church, J. A., Clark, P. U., Cazenave, A., Gregory, J. M., Jevrejeva, S., Levermann, A., Merrifield, M. A., Milne, G. A., Nerem, R. S., Nunn, P. D., Payne, A. J., Pfeffer, W. T., Stammer, D., & Unnikrishnan, A. S. (2013). *Sea level change* [Technical Report]. P.M.Cambridge University Press. http://drs.nio.org/drs/handle/2264/4605

Coles, S. (2001). *An Introduction to Statistical Modeling of Extreme Values*. Springer.

Douglas, E., Kirshen, P., DeConto, R. M., FitzGerald, D. M., Hay, C., Hughes, Z., Kemp, A. C., Kopp, R. E., Anderson, B., Kuang, Z., Ravela, S., Woodruff, J. D., Barlow, M., Collins, M., DeGaetano, A., Schlosser, C. A., Ganguly, A., Kodra, E., & Ruth, M. (2016). *Climate change and sea level rise projections for Boston: The Boston Research Advisory Group* *report.* (p. 54). Climate Ready Boston. https://www.boston.gov/sites/default/files/document-file-12-2016/brag_report_-_final.pdf

Eliot, M. (2010). Influence of interannual tidal modulation on coastal flooding along the Western Australian coast. *Journal of Geophysical Research: Oceans*, *115*(C11). https://doi.org/10.1029/2010JC006306

Emanuel, K. A. (2013). Downscaling CMIP5 climate models shows increased tropical cyclone activity over the 21st century. *Proceedings of the National Academy of Sciences*, *110*(30), 12219–12224. https://doi.org/10.1073/pnas.1301293110

Familkhalili, R., Talke, S. A., & Jay, D. A. (n.d.). Tide-Storm Surge Interactions in Highly Altered Estuaries: How Channel Deepening Increases Surge Vulnerability. *Journal of Geophysical Research: Oceans*, *n/a*(n/a), e2019JC015286. https://doi.org/10.1029/2019JC015286

Ferro, C. A. T., & Segers, J. (2003). Inference for clusters of extreme values. *Journal of the Royal Statistical Society: Series B (Statistical Methodology)*, *65*(2), 545–556. https://doi.org/10.1111/1467-9868.00401

Galloway, G. E., Baecher, G. B., Plasencia, D., Coulton, K. G., Louthain, J., Bagha, M., & Levy, A. R. (2006). *Assessing the Adequacy of the National Flood Insurance Program's 1 Percent Flood Standard* (p. 197) [2001-2006 Evalulation of the National Flood Insurance Program]. http://s3-us-gov-west-1.amazonaws.com/dam-production/uploads/20130726-1602-20490-6095/nfip_eval_1_percent_standard.pdf

Garner, A. J., Mann, M. E., Emanuel, K. A., Kopp, R. E., Lin, N., Alley, R. B., Horton, B. J., DeConto, R. M., Donnelly, J. P., & Pollard, D. (2017). Impact of climate change on New York City's coastal flood hazard: Increasing flood heights from the preindustrial to 2300 CE. *Proceedings of the National Academy of Sciences*, *114*(45), 11861–11866. https://doi.org/10.1073/pnas.1703568114

Garrett, C. (1972). Tidal Resonance in the Bay of Fundy and Gulf of Maine. *Nature*, *238*(5365), 441–443. https://doi.org/10.1038/238441a0

Goddard, P. B., Yin, J., Griffies, S. M., & Zhang, S. (2015). An extreme event of sea-level rise along the Northeast coast of North America in 2009–2010. *Nature Communications*, *6*(1), 1–9. https://doi.org/10.1038/ncomms7346

Godin, G. (1993). On tidal resonance. *Continental Shelf Research*, *13*(1), 89–107. https://doi.org/10.1016/0278-4343(93)90037-X

Greenberg, D. A., Blanchard, W., Smith, B., & Barrow, E. (2012). Climate Change, Mean Sea Level and High Tides in the Bay of Fundy. *Atmosphere-Ocean*, *50*(3), 261–276. https://doi.org/10.1080/07055900.2012.668670

Griggs, G., Arvai, J., Cayan, D., DeConto, R. M., Fox, J., Fricker, H. A., Kopp, R. E., Tebaldi, C., & Whiteman, E. A. (2017). *Rising seas in California: An update on sea-level rise* *science*. (p. 71) [California Ocean Science Trust Tech. Rep.]. http://climate.calcommons.org/bib/rising-seas-california-update-sea-level-rise-science

Haigh, I. D., Eliot, M., & Pattiaratchi, C. (2011). Global influences of the 18.61 year nodal cycle and 8.85 year cycle of lunar perigee on high tidal levels. *Journal of Geophysical Research: Oceans*, *116*(C6). https://doi.org/10.1029/2010JC006645

Haigh, I. D., Nicholls, R., & Wells, N. (2010). A comparison of the main methods for estimating probabilities of extreme still water levels. *Coastal Engineering*, *57*(9), 838–849. https://doi.org/10.1016/j.coastaleng.2010.04.002

Haigh, I. D., Pickering, M. D., Green, J. A. M., Arbic, B. K., Arns, A., Dangendorf, S., Hill, D. F., Horsburgh, K., Howard, T., Idier, D., Jay, D. A., Jänicke, L., Lee, S. B., Müller, M., Schindelegger, M., Talke, S. A., Wilmes, S.-B., & Woodworth, P. L. (2020). The Tides They Are A-Changin': A Comprehensive Review of Past and Future Nonastronomical Changes in Tides, Their Driving Mechanisms, and Future Implications. *Reviews of Geophysics*, *58*(1), e2018RG000636. https://doi.org/10.1029/2018RG000636

Hallegatte, S., Green, C., Nicholls, R. J., & Corfee-Morlot, J. (2013). Future flood losses in major coastal cities. *Nature Climate Change*, *3*(9), 802–806. https://doi.org/10.1038/nclimate1979

Horsburgh, K. J., Williams, J. A., Flowerdew, J., & Mylne, K. (2008). Aspects of operational forecast model skill during an extreme storm surge event. *Journal of Flood Risk Management*, *1*(4), 213–221. https://doi.org/10.1111/j.1753-318X.2008.00020.x

Hunter, J. (2010). Estimating sea-level extremes under conditions of uncertain sea-level rise. *Climatic Change*, *99*(3), 331–350. https://doi.org/10.1007/s10584-009-9671-6

Kendall, M. G. (1938). A New Measure of Rank Correlation. *Biometrika*, *30*(1/2), 81–93. JSTOR. https://doi.org/10.2307/2332226

Kirshen, P., Knee, K., & Ruth, M. (2008). Climate change and coastal flooding in Metro Boston: Impacts and adaptation strategies. *Climatic Change*, *90*(4), 453–473. https://doi.org/10.1007/s10584-008-9398-9

Knutson, T. R., McBride, J. L., Chan, J., Emanuel, K., Holland, G., Landsea, C., Held, I., Kossin, J. P., Srivastava, A. K., & Sugi, M. (2010). Tropical cyclones and climate change. *Nature Geoscience*, *3*(3), 157–163. https://doi.org/10.1038/ngeo779

Kopp, R. E., Horton, R. M., Little, C. M., Mitrovica, J. X., Oppenheimer, M., Rasmussen, D. J., Strauss, B. H., & Tebaldi, C. (2014). Probabilistic 21st and 22nd century sea-level projections at a global network of tide-gauge sites. *Earth's Future*, *2*(8), 383–406. https://doi.org/10.1002/2014EF000239

Ku, L.-F., Greenberg, D. A., Garrett, C. J. R., & Dobson, F. W. (1985). Nodal Modulation of the Lunar Semidiurnal Tide in the Bay of Fundy and Gulf of Maine. *Science*, *230*(4721), 69–71. https://doi.org/10.1126/science.230.4721.69

Leadbetter, M. R. (1983). Extremes and local dependence in stationary sequences. *Zeitschrift Für Wahrscheinlichkeitstheorie Und Verwandte Gebiete*, *65*(2), 291–306. https://doi.org/10.1007/BF00532484

Leffler, K., & Jay, D. A. (2009). Enhancing tidal harmonic analysis: Robust (hybrid L1/L2) solutions. *Continental Shelf Research*, *29*(1), 78–88. https://doi.org/10.1016/j.csr.2008.04.011

Lin, N., Emanuel, K. A., Smith, J. A., & Vanmarcke, E. (2010). Risk assessment of hurricane storm surge for New York City. *Journal of Geophysical Research: Atmospheres*, *115*(D18). https://doi.org/10.1029/2009JD013630

Menéndez, M., & Woodworth, P. L. (2010). Changes in extreme high water levels based on a quasi-global tide-gauge data set. *Journal of Geophysical Research: Oceans*, *115*(C10). https://doi.org/10.1029/2009JC005997

Müller, M. (2012). The influence of changing stratification conditions on barotropic tidal transport and its implications for seasonal and secular changes of tides. *Continental Shelf Research*, *47*, 107–118. https://doi.org/10.1016/j.csr.2012.07.003

Müller, M., Cherniawsky, J. Y., Foreman, M. G. G., & Storch, J.-S. von. (2012). Global M2 internal tide and its seasonal variability from high resolution ocean circulation and tide modeling. *Geophysical Research Letters*, *39*(19). https://doi.org/10.1029/2012GL053320

Neumann, B., Vafeidis, A. T., Zimmermann, J., & Nicholls, R. J. (2015). Future Coastal Population Growth and Exposure to Sea-Level Rise and Coastal Flooding—A Global Assessment. *PLOS ONE*, *10*(3), e0118571. https://doi.org/10.1371/journal.pone.0118571

NYC. (2013). *A stronger, more resilient New York* (p. 435) [New York City PlaNYC Tech Rep.]. https://www1.nyc.gov/assets/sirr/downloads/pdf/Ch_2_ClimateAnalysis_FINAL_singles.pdf

Oppenheimer, M., Glavovic, B. C., Hinkel, J., van de Wal, R., Magnan, A. K., Abd-Elgawad, A., Cai, R., Cifuentes-Jara, M., DeConto, R. M., Ghosh, T., Hay, J., Isla, F., Marzeion, B., Meyssignac, B., & Sebesvari, Z. (n.d.). *Sea Level Rise and Implications for Low-Lying Islands, Coasts and Communities.* (IPCC Special Report on the Ocean and Cryosphere in a Changing Climate).

Pawlowicz, R., Beardsley, B., & Lentz, S. (2002). Classical tidal harmonic analysis including error estimates in MATLAB using T_TIDE. *Computers & Geosciences*, *28*(8), 929–937. https://doi.org/10.1016/S0098-3004(02)00013-4

Pelling, H. E., & Green, J. A. M. (2013). Sea level rise and tidal power plants in the Gulf of Maine. *Journal of Geophysical Research: Oceans*, *118*(6), 2863–2873. https://doi.org/10.1002/jgrc.20221

Peng, D., Hill, E. M., Meltzner, A. J., & Switzer, A. D. (2019). Tide Gauge Records Show That the 18.61-Year Nodal Tidal Cycle Can Change High Water Levels by up to 30 cm. *Journal of Geophysical Research: Oceans*, *124*(1), 736–749. https://doi.org/10.1029/2018JC014695

Pugh D. T., & Vassie J. M. (1978). Extreme Sea Levels from Tide and Surge Probability. *Coastal Engineering 1978*, 911–930. https://doi.org/10.1061/9780872621909.054

Pugh, D., & Vassie, J. (1980). Applications of the joint probability method for extreme sea level computations. *Proceedings of the Institution of Civil Engineers*, *69*(4), 959–975. https://doi.org/10.1680/iicep.1980.2179

Ray, R. D. (2006). Secular changes of the M2 tide in the Gulf of Maine. *Continental Shelf Research*, *26*(3), 422–427. https://doi.org/10.1016/j.csr.2005.12.005

Ray, R. D., & Merrifield, M. A. (2019). The Semiannual and 4.4-Year Modulations of Extreme High Tides. *Journal of Geophysical Research: Oceans*, *124*(8), 5907–5922. https://doi.org/10.1029/2019JC015061

Ray, R. D., & Talke, S. A. (2019). Nineteenth-Century Tides in the Gulf of Maine and Implications for Secular Trends. *Journal of Geophysical Research: Oceans*, *124*(10), 7046–7067. https://doi.org/10.1029/2019JC015277

Ray, Richard D., & Foster, G. (2016). Future nuisance flooding at Boston caused by astronomical tides alone. *Earth's Future*, *4*(12), 578–587. https://doi.org/10.1002/2016EF000423

Schindelegger, M., Green, J. a. M., Wilmes, S.-B., & Haigh, I. D. (2018). Can We Model the Effect of Observed Sea Level Rise on Tides? *Journal of Geophysical Research: Oceans*, *123*(7), 4593–4609. https://doi.org/10.1029/2018JC013959

Talke, S. A., Kemp, A. C., & Woodruff, J. (2018). Relative Sea Level, Tides, and Extreme Water Levels in Boston Harbor From 1825 to 2018. *Journal of Geophysical Research: Oceans*, *123*(6), 3895–3914. https://doi.org/10.1029/2017JC013645

Talke, S. A., Mahedy, A., Jay, D. A., Lau, P., Hilley, C., & Hudson, A. (2020). Sea Level, Tidal, and River Flow Trends in the Lower Columbia River Estuary, 1853–present. *Journal of Geophysical Research: Oceans*, *125*(3), e2019JC015656. https://doi.org/10.1029/2019JC015656

Talke, Stefan A, & Jay, D. A. (2020). Changing Tides: The Role of Natural and Anthropogenic Factors. *Annual Review of Marine Science*, *12*, 121–151. https://doi.org/10.1146/annurev-marine-010419-010727

Tawn, J. A., & Vassie, J. M. (1989). *Extreme Sea Levels: the Joint Probabilities Method Revisited and Revised*. https://trid.trb.org/view/435293

Tawn, Jonathan A. (1992). Estimating Probabilities of Extreme Sea-Levels. *Journal of the Royal Statistical Society: Series C (Applied Statistics)*, *41*(1), 77–93. https://doi.org/10.2307/2347619

Tebaldi, C., Strauss, B. H., & Zervas, C. E. (2012). Modelling sea level rise impacts on storm surges along US coasts. *Environmental Research Letters*, *7*(1), 014032. https://doi.org/10.1088/1748-9326/7/1/014032

Thompson, P. R., Mitchum, G. T., Vonesch, C., & Li, J. (2013). Variability of Winter Storminess in the Eastern United States during the Twentieth Century from Tide Gauges. *Journal of Climate*, *26*(23), 9713–9726. https://doi.org/10.1175/JCLI-D-12-00561.1

Vousdoukas, M. I., Voukouvalas, E., Mentaschi, L., Dottori, F., Giardino, A., Bouziotas, D., Bianchi, A., Salamon, P., & Feyen, L. (2016). Developments in large-scale coastal flood hazard mapping. *Natural Hazards and Earth System Sciences*, *16*(8), 1841–1853. https://doi.org/10.5194/nhess-16-1841-2016

Wahl, T., Haigh, I. D., Nicholls, R. J., Arns, A., Dangendorf, S., Hinkel, J., & Slangen, A. B. A. (2017). Understanding extreme sea levels for broad-scale coastal impact and adaptation analysis. *Nature Communications*, *8*(1), 1–12. https://doi.org/10.1038/ncomms16075

Wahl, Thomas, & Chambers, D. P. (2015). Evidence for multidecadal variability in US extreme sea level records. *Journal of Geophysical Research: Oceans*, *120*(3), 1527–1544. https://doi.org/10.1002/2014JC010443

Williams, J., Horsburgh, K. J., Williams, J. A., & Proctor, R. N. F. (2016). Tide and skew surge independence: New insights for flood risk. *Geophysical Research Letters*, *43*(12), 6410–6417. https://doi.org/10.1002/2016GL069522

Winterwerp, J. C., Wang, Z. B., van Braeckel, A., van Holland, G., & Kösters, F. (2013). Man-induced regime shifts in small estuaries—II: A comparison of rivers. *Ocean Dynamics*, *63*(11), 1293–1306. https://doi.org/10.1007/s10236-013-0663-8

Wolf, J. (2008). Coupled wave and surge modelling and implications for coastal flooding. *Advances in Geosciences*, *17*, 19–22. https://doi.org/10.5194/adgeo-17-19-2008

Wolf, Judith. (2009). Coastal flooding: Impacts of coupled wave–surge–tide models. *Natural Hazards*, *49*(2), 241–260. https://doi.org/10.1007/s11069-008-9316-5

Woodworth, P. L. (2010). A survey of recent changes in the main components of the ocean tide. *Continental Shelf Research*, *30*(15), 1680–1691. https://doi.org/10.1016/j.csr.2010.07.002

Zervas, C. (2013). *Extreme Water Levels of the United States 1893-2010* (NOAA Technical Report NOS CO-OPS 067; p. 200). NOAA. https://tidesandcurrents.noaa.gov/publications/NOAA_Technical_Report_NOS_COOPS_067a.pdf

Table 1. Gulf of Maine NOAA tide gauge station info.

Station; NOAA station no.	**Approximate location**	**Timespan**	**Mean high water (m)[a]**	**Mean higher high water (m)[a]**	**Great diurnal range (m)[a]**
Eastport, ME; 8410140	44°54.2'N 66°59.1'W	1929–present	2.771	2.916	5.874
Portland, ME; 8418150	43°39.3'N 70°14.8'W	1910–present	1.380	1.513	3.019
Boston, MA; 8443970	42°21.2'N 71°3.0'W	1921–present	1.411	1.545	3.131

[a] Tidal datums are relative to 1983-2001 mean sea level

Table 2. Results of Kendall's tau correlation test, using the top 1% of skew surges and their associated predicted high waters.

	Summer		**Winter**	
	tau	**p-value**	**tau**	**p-value**
Eastport	0.02	0.59	-0.02	0.58
Portland	-0.01	0.80	-0.08	0.03
Boston	0.05	0.14	0.01	0.75

Table 3. Ranges of 18.6 and 4.4-year tidal cycle modulations of the 1% AEP storm tide ($ST_{1\%}$) and the highest predicted tide.

	18.6-year modulation range (mm)		**quasi 4.4-year modulation range (mm)**	
	$ST_{1\%}$	**highest predicted tide**	**$ST_{1\%}$**	**highest predicted tide**
Eastport	126	196	28	78
Portland	37	66	37	68
Boston	55	72	28	62